Risk of myocardial infarction based on endothelial shear stress analysis using coronary angiography

(Article begins on next page)

04 October 2023

1 **Risk of Myocardial Infarction based on Endothelial Shear Stress Analysis Using**
2 **Coronary Angiography**
3
4 Running title: Endothelial shear stress predicts myocardial infarction.
5 Total word count (main text including legends to figures and tables): 3'796 words.
6 Number of figures and/or tables: 3 figures and 2 tables.
7 Number of references: 28.
8

9 Alessandro Candreva, MD[a,b], Mattia Pagnoni, MD[c], Maurizio Lodi Rizzini, MS[d], Takuya
10 Mizukami, MD, PhD[a,e], Emanuele Gallinoro, MD[a,f], Valentina Mazzi, MS[d], Diego Gallo,
11 PhD[d], David Meier, MD[c], Toshiro Shinke, MD,PhD[e], Jean-Paul Aben, MSc[g], Sakura
12 Nagumo, MD[a,e], Jeroen Sonck, MD[a,h], Daniel Munhoz MD, PhD[a,h,i], Stephane Fournier,
13 MD[c,h], Emanuele Barbato MD, PhD[a,h], Ward Heggermont, MD, PhD[a], Stephane Cook, MD[j],
14 Claudio Chiastra, PhD[d], Umberto Morbiducci, PhD[d], Bernard De Bruyne, MD, PhD[a,c], Oliver
15 Muller, MD, PhD[c], and Carlos Collet, MD, PhD[a*]
16
17 [a] Cardiovascular Center Aalst, OLV-Clinic, Aalst, Belgium
18 [b] Dept. of Cardiology, Zurich University Hospital, Zurich, Switzerland
19 [c] Dept. of Cardiology, Lausanne University Hospital, Lausanne, Switzerland
20 [d] Dept. of Mechanics, Politecnico di Torino, Turin, Italy
21 [e] Dept. of Cardiology, Showa University School of Medicine, Tokyo, Japan
22 [f] Dept. of Translational Medical Sciences, University of Campania 'Luigi Vanvitelli', Naples, Italy
23 [g] Pie Medical Imaging BV, Maastricht, The Netherlands
24 [h] Dept. of Advanced Biomedical Sciences, University of Naples Federico II, Naples, Italy
25 [i] Department of internal medicine, University of Campinas (Unicamp), Campinas, Brazil.
26 [j] Department of Cardiology, HFR Fribourg, Fribourg, Switzerland
27 [*] Corresponding author
28
28 **Address for correspondence:**
29 Carlos Collet Bortone, MD, PhD
30 Cardiovascular Center Aalst, OLV-Clinic, Aalst, Belgium.
31 Moorselbaan, 1654, B-9300 Aalst; Phone: +32 53 72 44 39;
32 e-mail: carloscollet@gmail.com
33
34

1 **Abstract**
2 Background and aims: Wall shear stress (WSS) has been associated with atherogenesis
3 and plaque progression. The present study assessed the value of WSS analysis derived from
4 conventional coronary angiography to detect lesions culprit for future myocardial infarction
5 (MI).
6 Methods and Results: Three-dimensional quantitative coronary angiography (3DQCA),
7 was used to calculate WSS and pressure drop in 80 patients. WSS descriptors were compared
8 between 80 lesions culprit of future MI and 108 non-culprit lesions (controls). Endothelium-
9 blood flow interaction was assessed by computational fluid dynamics (10.8 ± 1.41 min per
10 vessel). Median time between the baseline angiography and MI was 25.9 (21.9-29.8) months.
11 Mean patient age was 70.3 ± 12.7. Clinical presentation was STEMI in 35% and NSTEMI in
12 65%. Culprit lesions showed higher percent area stenosis (%AS), translesional vFFR difference
13 (ΔvFFR), time-averaged WSS (TAWSS) and topological shear variation index (TSVI)
14 compared to non-culprit lesions ($p<0.05$ for all). TSVI was superior to TAWSS in predicting
15 MI (AUC-TSVI=0.77, 95%CI 0.71-0.84 vs. AUC-TAWSS=0.61, 95%CI 0.53-0.69, $p<0.001$).
16 The addition of TSVI increased predictive and reclassification abilities compared to a model
17 based on %AS and ΔvFFR (NRI=1.04, p<0.001, IDI=0.22, $p<0.001$).
18 Conclusions: A 3DQCA-based WSS analysis was feasible and can identify lesions
19 culprit for future MI. The combination of area stenoses, pressure gradients and WSS predicted
20 the occurrence of MI. TSVI, a novel WSS descriptor, showed strong predictive capacity to
21 detect lesions prone to cause MI.
22
23 **Highlights:**
24 • Lesions culprit of future MI had higher area stenoses, pressure gradients, TAWSS and
25 TSVI.
26 • A 3DQCA-based software provided in few minutes reliable WSS simulations.
27 • The novel WSS-based descriptor TSVI showed strong predictive capacity for future MI.
28
32
33

Abbreviations:

%AS	Percent area stenosis	MLD	Minimal lumen diameter
CABG	Coronary artery bypass graft	NCL	Non-culprit lesion
CAD	Coronary artery disease	QCA	Quantitative coronary angiography
CFD	Computational fluid dynamics	TSVI	Topological shear variation index
FCL	Future culprit lesion	vFFR	Virtual fractional flow reserve
FFR	Fractional flow reserve	WSS	Wall shear stress
MI	Myocardial infarction		

34

1   **Graphical Abstract – Risk of myocardial infarction based on endothelial shear stress**

2   **analysis using coronary angiography.**

3
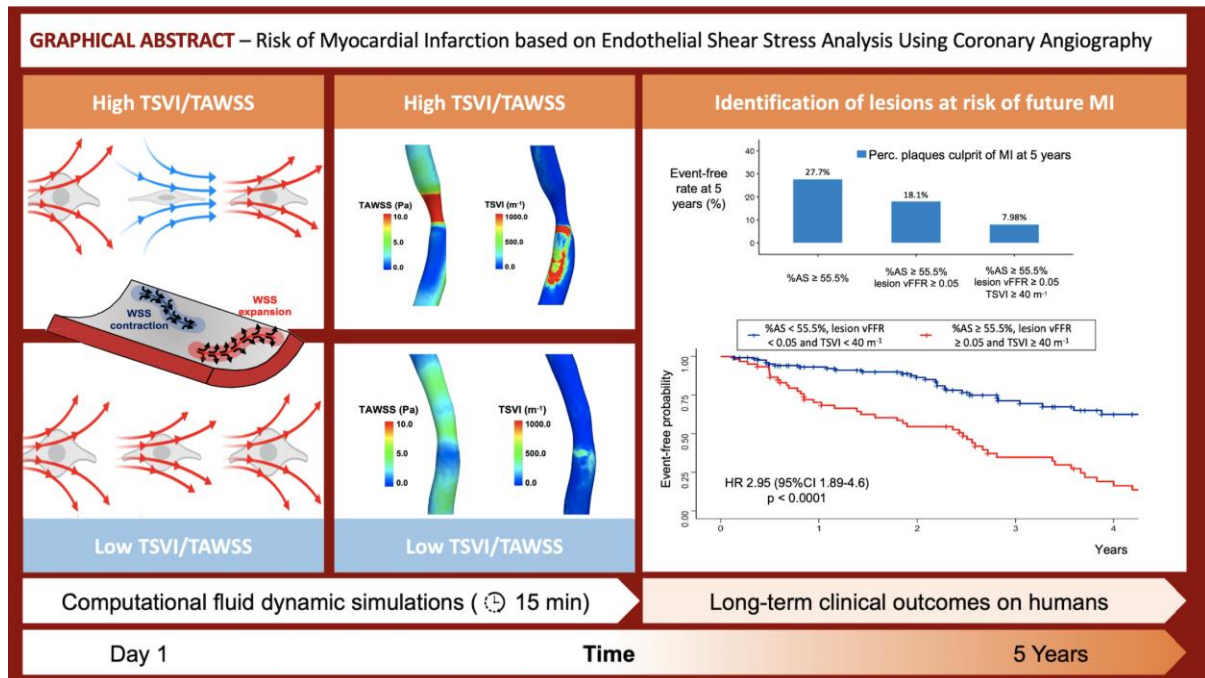
4

5

6   Shear forces acting on endothelial surface can be simulated with computational fluid dynamics-

7   based software from conventional coronary angiograms. The variability of local

8   contraction/expansion action exerted by shear forces along the cardiac cycle is captured by the

9   topological shear variation index (TSVI, in m^{-1}), while the time-averaged wall shear stress

10   (TAWSS, in Pa) describes their averaged magnitude along the cardiac cycle. Both WSS-based

11   descriptors identified lesions culprit of myocardial infarction at 5 year, however TSVI could

12   significantly further improve predictivity, reclassification and discriminatory capacity when

13   added to percentage area stenosis (%AS) and translesional difference in the virtual fractional

14   flow reserve (ΔvFFR).

1   **Introduction**

2   Coronary arteries – and atherosclerotic plaques – experience a variety of mechanical

3   forces linked to plaque progression and destabilization.[1, 2] Among them, high pressure

4   gradients across epicardial lesions have been recognized as independent predictors of

5   myocardial infarction (MI).[3] The frictional force of the flowing blood acting on the

6   endothelium, i.e. wall shear stress (WSS), is also a key mechanism translating hemodynamic

7   signals to vascular biological phenomena.[4, 5] In addition, WSS has been associated with

8   vulnerable transformation of atherosclerotic lesions: low WSS has been linked to

9   atherosclerosis progression, whereas high WSS has been associated with platelet activation and

10   plaque rupture.[6, 7] More recently, WSS-based descriptors able to characterize the

11   contraction/expansion action of endothelial shear forces along the cardiac cycle were

12   associated with vascular pathophysiological processes in coronary and extra-coronary

13   territories.[8-10] In particular, a recent longitudinal study on swine models showed that early

14   atherosclerotic changes in coronary arteries are associated with the endothelium shear stress

15   contraction/expansion variability along the cardiac cycle, captured by the WSS-based quantity

16   topological shear variation index (TSVI).[10]

17   The present study evaluates the efficacy of an anatomical and hemodynamic assessment

18   based on computational fluid dynamic (CFD) simulations, obtained from conventional

19   coronary angiography for the identification of lesions prone to cause MI within five years.

1   **Materials and Methods**

2   *Study design*

3   This is a case-control multicenter study including three European centers (OLV clinic,

4   Aalst, Belgium; University of Lausanne, Switzerland; Fribourg Cantonal Hospital,

5   Switzerland) designed to identify predictors of MI. Study protocol conforms to the ethical

6   guidelines of the 1975 Declaration of Helsinki and has been approved by the Institution's ethics

7   committee. Written informed consent was obtained from each patient included in the study.

8   *Study population*

9   Patients presenting with acute MI admitted for invasive coronary angiography were

10   screened to identify those who (i) had a previous coronary angiography (here forth referred as

11   baseline angiography) performed between 1 month and 5 years before the index event, (ii) had

12   the visually identifiable mild lesion ($\leq 50\%$ visual diameter stenosis) culprit for the future MI

13   at the baseline angiography, and (iii) had at the baseline angiography at least one additional

14   non-culprit lesion (NCL) in at least one of the other two major epicardial vessels. Therefore,

15   each patient served as its own control. Patient exclusion criteria were post-coronary artery

16   bypass graft (CABG) status, MI as result of in-stent restenosis or thrombosis, MI in absence of

17   angiographically identifiable coronary lesions, ostial lesions or lesions involving a coronary

18   bifurcation with a side branch diameter ≥ 2 mm. In case of multiple coronary angiographies

19   before the acute event, the latest angiography was selected for analysis.

20   Lesion selection (for both future culprit lesions, FCL, and NCL) was performed blinded

21   to the information of which lesion evolved towards an MI. Subsequently, three-dimensional

1   geometries derived from coronary angiography of both FCL and NCL were generated for blood

2   flow simulations.

3   *Coronary angiography and blood flow simulations*

4   The workflow of the study is presented in **Figure 1**. Three-dimensional quantitative

5   coronary angiography (3DQCA) reconstructions were performed using two angiographic end-

6   diastolic frames at least 30 degrees apart using the CAAS Workstation WSS software (Pie

7   Medical Imaging, Maastricht, the Netherlands). Automated lumen contour detection was

8   enabled, and manually corrected when needed. Three-dimensional coronary reconstruction

9   included at least 20 mm proximally and 20 mm distally from the minimal lumen diameter

10   (MLD). Using the three-dimensional coronary reconstruction, CFD simulations were carried

11   out automatically using a finite element-based code (CAAS Workstation WSS software) to

12   quantify WSS distribution along the cardiac cycle under resting conditions. Details on

13   numerical settings are reported in the **Supplemental Methods**. Simulations were performed

14   on a standard computer with processor Intel Xeon W-2123, 3.6GHz, 4 cores, RAM 16Gb.

15   3DQCA and the angiography-derived virtual fractional flow reserve (vFFR) were

16   obtained using the CAAS Workstation vFFR software (Pie Medical Imaging) on the same

17   angiographic projections selected for three-dimensional vessels reconstruction. Anatomical

18   descriptors included percentage area stenosis (%AS), percentage diameter stenosis, minimal

19   lumen area (MLA) and diameter, reference vessel diameter, lesion length and distance of MLA

20   from the ostium. The distal vFFR, the translesional vFFR difference (ΔvFFR), and the absolute

21   pressure drop in millimeters of mercury (mmHg) at the distal part of the vessel, i.e. distal

22   pressure gradient, were extracted as detailed elsewhere.[11]

1   *Wall shear stress descriptors*

2   The quantitative characterization of endothelial shear forces included the following

3   WSS-based descriptors (**Supplemental Table 1**): time-averaged wall shear stress (TAWSS),

4   obtained by averaging the local values of WSS magnitude along the cardiac cycle

5   (**Supplemental Figure 1**);[12] oscillatory shear index (OSI);[13] transverse WSS (transWSS);[14]

6   TAWSS axial component ($TAWSS_{ax}$) and secondary component ($TAWSS_{sc}$);[15] relative

7   residence time (RRT);[16] and topological shear variation index (TSVI).[8-10] The next paragraph

8   further expands on TSVI.

9   Endothelial contraction/expansion regions can be mathematically identified analyzing

10   the WSS topological skeleton, in particular through negative/positive local values of the

11   divergence of the WSS unit vector field (DIV_{WSS}).[17] Technically, the variability of DIV_{WSS}

12   along the cardiac cycle can be measured using the WSS-based quantity TSVI [17] (**Supplemental**

13   **Figure 2** and **Supplemental Movie**), defined as the root mean square deviation of the

14   instantaneous divergence of the unit WSS vector field with respect to its average over the

15   cardiac cycle:

16   $$\mathrm{TSVI} = \left\{ \frac{1}{T} \int_0^T [\mathrm{DIV_{WSS}} - \overline{\mathrm{DIV_{WSS}}}]^2 dt \right\}^{1/2}, \quad (\text{Eq. 1})$$

17   where T is the duration of the cardiac cycle and the overbar denotes a cycle-average quantity.

18   Theoretical and technical details on the method of analysis of the WSS topological skeleton

19   here adopted have been exhaustively reported elsewhere.[17]

20   The WSS-based descriptors are presented as averaged or maximum and minimum

21   values over three distinct vessel segments: (i) lesion, defined as the segment including the MLA

22   and delimited proximally and distally by the intersection of the QCA diameter function line

1   with the interpolated reference line, (ii) an upstream segment with a length of three times the

2   diameter of the proximal boundary of the lesion, and (iii) a downstream segment with a length

3   of three times the diameter of the distal boundary of the lesion, to ensure a consistent spatial

4   extent across all cases (**Supplemental Figure 3**).

5   To assess reliability, CFD simulations carried out by physicians (AC) in standard

6   clinical settings (hence denoted as 'clinical CFD') using the CAAS Workstation WSS software

7   were tested against state-of-the-art simulations carried out by experts in computational

8   hemodynamics (MLR, VM, DG, CCh, UM) with higher resolution and numerical robustness

9   ('expert CFD'), as further detailed in **Supplemental Methods**. The capability of WSS-based

10   quantities to discriminate FCL vs. NCL groups was tested for both clinical and expert CFD.

11   To assess the reproducibility of the WSS evaluation process, thirty coronary arteries

12   were randomly selected and WSS simulations were repeated with the same software.

13   *Statistical Methods*

14   All statistical analyses were performed on a per-lesion basis to compare FCL and NCL

15   characteristics. Continuous variables with normal distribution are presented as mean±standard

16   deviation (SD) and non-normally distributed variables as median (inter-quartile range [IQR]).

17   Categorical variables are presented as percentages. Chi-squared test was used for comparing

18   categorical variables, while Student's tests (or Mann-Whitney tests as appropriate) for

19   continuous ones. A p-value <0.05 was considered significant. The predictive capacity of QCA-

20   , vFFR- and WSS-based descriptors was assessed using C-statistics. Receiving operator

21   characteristic (ROC) curve were compared using the DeLong method.[18] To determine the net

22   reclassification index (NRI) and relative integrated discrimination improvement (IDI) for each

1   model, continuous variables were dichotomized according to optimal cut-off values from the

2   ROC curves. Three models were defined: the anatomical model (based on %AS) (model 1),

3   the anatomical and pressure model (based on %AS and ΔvFFR) (model 2), and a third model

4   based on %AS, ΔvFFR and a WSS descriptor (model 3). Time-to-event data are presented as

5   Kaplan-Meier estimates. Anatomical and functional variables presenting a univariate

6   relationship with future MI entered the multivariate Cox proportional-hazards regression

7   models. Associated risk for discrete increments was assessed with odds ratio (OR) derived

8   from binary logistic regression. WSS-based quantities reproducibility was assessed with

9   intraclass correlation coefficients (ICC). All analyses were performed using R statistical

10 software (R Foundation for Statistical Computing, Vienna, Austria).

11

1   **Results**

2   *Patient selection*

3   From January 2008 to December 2019, 6885 patients underwent coronary

4   catheterization for acute MI in the three participating centers, 775 (11.3%) patients had a

5   previous angiography, among which 80 (vessel n=190; 2.37±0.47 vessel/patient) were included

6   (the sequential screening steps for clinical and analytical exclusion criteria are summarized in

7   **Supplemental Figure 4)**. Clinical characteristics of the selected patients are summarized in

8   **Table 1**. At the time of the MI, mean age of patients was 70.3±12.7 years, 28.7% were female

9   and 76.3% were on Aspirin and 90.0% on statins. Non-ST elevation myocardial infarction

10   (NSTEMI) and STEMI were reported in 65% and 35% of the studied patients, respectively.

11   Percutaneous coronary intervention was performed in 97.5% (78/80) of cases. The culprit

12   lesion was located in the LAD in 43.8% of cases, in the LCX in 28.7% of cases and in the RCA

13   in 27.5% of cases. Median time between baseline and index angiography was 25.9 (IQR 21.9-

14   29.8) months. The angiography-based analysis of QCA, vFFR and WSS was equally feasible

15   in 98.9% of vessels (188 vessels, of which FCL n=80, NCL n=108).

16   *Anatomical and functional parameters and risk for subsequent myocardial infarction*

17   Percent AS was significantly higher in the FCL group (63.1±12.4 vs. 55.8±12.5,

18   *p*<0.001). Distal vFFR was lower in FCL compared to NCL (0.84 (IQR 0.75-0.90) vs. 0.86

19   (IQR 0.82-0.92), *p*=0.009); whereas ΔvFFR was higher in FCL compared to NCL (0.08 (IQR

20   0.04-0.13) vs. 0.05 (IQR 0.03-0.08), *p*=0.002) with a pressure drop across the lesion of 14.5

21   (IQR 9.0-22.5) mmHg in FCL vs. 12.0 (IQR 8.0-16.0) mmHg in NCL (*p*=0.012; **Table 2**).

22   %AS and ΔvFFR emerged as moderate independent predictors for MI (%AS AUC 0.65, 95%CI

1   0.57-0.73, $p<0.001$ and ΔvFFR AUC 0.63, 95%CI 0.55-0.71, $p<0.001$), with best cut-off

2   values derived from ROC curves analysis equal to 55.5% for %AS and 0.05 for ΔvFFR

3   (**Supplemental Table 2**).

4   *Wall shear stress descriptors and risk for future myocardial infarction*

5   On average, the computational time per clinical CFD-based WSS analysis was

6   10.8 ± 1.41 min.

7   Differences in the distribution of WSS-based quantities between the FCL and NCL

8   groups at the lesion level are reported in **Supplemental Figure 5**, while comparison of the heat

9   maps of WSS-based quantities as obtained from the two CFD approaches are presented in

10   **Supplemental Figure 6**. OSI average values were a scale factor of ten lower than the OSI

11   upper bound value (by construction, $0\leq OSI\leq0.50$), and on average approximated zero. For this

12   reason, OSI was not considered in the further analyses.

13   Results of the univariate analysis are reported in **Supplemental Table 2**. Both TAWSS

14   and TSVI values were significantly higher in the FCL group at the level of the lesion segment

15   (4.58 Pa in FCL vs. 3.38 Pa in NCL, $p=0.01$ and 89.00 m^{-1} in FCL vs 49.10 m^{-1} in NCL,

16   $p<0.001$, respectively, **Supplemental Table 3**). The ROC curves analysis of TAWSS and

17   TSVI, evaluated at the lesion level, showed moderate and high predictive capacity for MI

18   (TAWSS AUC 0.61, 95%CI 0.53-0.69, $p=0.003$; TSVI AUC 0.77, 95%CI 0.71-0.84, $p<0.001$),

19   respectively. The best cut-off values were to 5.01 Pa and 40.50 m^{-1} for TAWSS and TSVI,

20   respectively. The capacity of TSVI to predict the clinical outcome MI was markedly higher

21   than TAWSS (**Figure 2** and **Supplemental Figure 7**). This was also confirmed when

22   evaluating predictive capacity separately for NSTEMI (TAWSS AUC 0.63, 95%CI 0.53-0.73,

1   *p*=0.007; TSVI AUC 0.74, 95%CI 0.66-0.83, *p*<0.001) and STEMI (TAWSS AUC 0.58,

2   95%CI 0.44-0.72, *p*=0.131; TSVI AUC 0.83, 95%CI 0.73-0.93, *p*<0.001).

3   The reproducibility of the CFD-based WSS analyses quantities was excellent (TAWSS

4   ICC 0.98, 95%CI 0.95-0.99 and TSVI ICC 0.96, 95%CI 0.91-0.98), **Supplemental Figure 8**).

5   *Multivariable predictive models for myocardial infarction*

6   Compared with the anatomical model with %AS (model 1), the inclusion of ΔvFFR

7   (model 2), while not adding predictive capacity (model 1: AUC 0.65, 95%CI 0.57-0.73; model

8   2: AUC 0.66, 95%CI 0.58-0.74; *p*=0.460), led to a significant improvement in the

9   reclassification and in the discrimination capacity (NRI 0.53, 95%CI 0.25-0.80, *p*<0.001;

10   relative IDI 0.03, 95%CI 0.001-0.05, *p*=0.020) for the identification of lesions culprit of

11   subsequent MI. Similarly, the addition of TAWSS (model 3 based on TAWSS) led to a non-

12   significant increase in the predictive capacity of the model for detecting FCL (model 2: AUC

13   0.66, 95%CI 0.58-0.74; model 3 based on TAWSS: AUC 0.69, 95%CI 0.61-0.76; *p*=0.099)

14   with a significant improvement in the reclassification capacity and discriminatory gain (NRI

15   0.45, 95%CI 0.21-0.69, *p*<0.001; relative IDI 0.04, 95%CI 0.01-0.07, *p*=0.008). On the

16   contrary, the addition of TSVI to the anatomical and pressure model, led to a significant

17   increase in predictive capacity for MI (model 2: AUC 0.66, 95%CI 0.58-0.74; model 3 based

18   on TSVI: AUC 0.77, 95%CI 0.70-0.84; *p*<0.001; **Supplemental Figure 9** and **Supplemental**

19   **Table 4**) with incremental reclassification and discriminatory capacity (NRI 1.04, 95%CI 0.81-

20   1.27, *p*<0.001; relative IDI 0.22, 95%CI 0.16-0.27, *p*<0.001; **Supplemental Tables 5** and **6**).

21   *Time-to-event analysis*

1   Event-free probabilities were investigated for %AS, ΔvFFR, TAWSS and TSVI

2   (**Figure 3, Supplemental Figures 10** and **11**). The single strongest predictor of MI at the lesion

3   level was TSVI (HR 5.11, 95%CI 2.70-9.68, *p*<0.001; **Supplemental Table 7**). An increment

4   of TSVI of 100 m^{-1} was associated with six-fold increased odds for a future MI (OR 5.97,

5   95%CI 2.94-13.5; **Supplemental Figure 12**).

1   **Discussion**

2   The present study proved that a comprehensive approach based on a novel 3DQCA

3   software is able to identify lesions culprit of future MI. The main findings of the study can be

4   summarized as follows: (i) a 3DQCA-based software was able to provide in few minutes

5   reliable WSS-based quantities from CFD simulations from standard angiographic images; ii)

6   FCL had higher area stenoses, higher pressure gradients, and higher TAWSS and TSVI values

7   than the control lesions; (iii) a model integrating anatomical, pressure and WSS descriptors

8   showed improved discriminatory and reclassification capacity in identifying lesions culprit of

9   future MI compared with a model based on anatomy and pressure gradients alone; (iv) a

10   recently introduced WSS-based descriptor measuring the variability of the

11   contraction/expansion action exerted by the WSS on the endothelium along the cardiac cycle,

12   TSVI, [19] exhibited strong predictive capacity for future MI.

13   Studies based on intravascular imaging led to the identification of several markers of

14   plaque vulnerability.[20, 21] Nevertheless, the vast majority of these 'high-risk plaques' become

15   quiescent over time, thus challenging the vulnerable plaque concept.[20] On the other hand, since

16   mild lesions outnumber severe stenoses, a sizable proportion of MI occurs at the site of mild

17   lesions.[19] Using coronary computed tomography angiography (CCTA) the EMERALD study

18   demonstrated the added value of the integration of hemodynamic features with plaque

19   characteristic to identify lesions prone to rupture.[22] Pursuing a similar aim, the present study

20   combined angiographic information with translesional pressure and WSS-based quantities.

21   Lesions were classified as culprit and non-culprit according to an overt clinical event, and NCL

22   served as internal control, thus accounting for the intrinsic biological variability. In contrast to

1   previous studies, the culprit criterion referred to a clinically relevant endpoint (i.e. MI), thus

2   minimizing biases related to softer endpoints, such as anatomical plaque progression or target

3   vessel revascularization.[23, 24]

4   *Applicability and reliability of CFD simulations based on conventional angiography*

5   Based on recent studies confirming the reliability of angiographically-derived WSS,[25]

6   the present work nurtured from the combination of conventional coronary angiography and

7   CFD algorithms, allowing for a multidimensional lesion evaluation. Despite this complexity, a

8   remarkable clinical implication of the present study is that all analyses were obtained by a

9   clinician in 10.8±1.41 minutes from conventional angiography using a standard computer.

10 Hence, the methodological approach offered in the present study brings WSS and derived

11 quantities closer to the clinical environment, where otherwise CFD simulations require

12 substantial computational efforts, and in most cases mandate the support of experts.

13 To further legitimate the clinical application of the investigated clinical CFD approach,

14 the reliability for WSS calculation was tested against simulations with higher resolution and

15 numerical robustness carried out by experts in computational hemodynamics. The reliability

16 of the clinical CFD approach was tested in terms of statistical significance rather than as

17 reproducibility at the single-node level of computational grids. The comparison of the heat

18 maps of WSS-based quantities as obtained from the two CFD approaches (**Supplemental**

19 **Figure 6**) highlighted that the clinical CFD is adequately robust to replicate the results obtained

20 using expert CFD, in terms of MI predictivity. The clinical CFD allowed for a WSS calculation

21 in shorter times without substantial loss in WSS predictive strength of MI.

22

1

2   *Inclusion of computational hemodynamics for MI prediction*

3   Anatomical lesion severity and translesional vFFR had a significant albeit modest

4   capacity of detecting lesions culprit of future MI (**Supplemental table 5**). For this reason, this

5   study also investigated the action of shear forces at the blood-endothelium interface. Previous

6   studies have shown that low TAWSS (<1.50 Pa) was associated with endothelial dysfunction

7   and plaque progression,[6] while high TAWSS (>4.71 Pa) in the proximal segments of the

8   atherosclerotic plaque was predictive of plaque disruption and MI.[7] More recently, a maximal

9   TAWSS above 4.95 Pa over 3 mm vascular segment independently predicted adverse

10 cardiovascular events requiring revascularization.[25] A significant association between TAWSS

11 and the occurrence of MI was confirmed also in the present study (p=0.011), and in line with

12 previous findings TAWSS significantly predicted MI, albeit weakly (TAWSS AUC 0.61,

13 95%CI 0.53-0.69, p=0.003). Moreover, the TAWSS cutoff (i.e. 5.01 Pa) supports previous

14 reports.[7] However, in contrast with the EMERALD study and the FAME 2 WSS sub-analysis,[7,

15 [22] the present study cohort had a lower functional lesion severity as depicted by the proportion

16 of hemodynamically significant lesions (19.7% vs. 49.0% vs. 100.0% in the current study,

17 EMERALD and FAME 2, respectively). Finally, vessels with borderline FFR values (0.81-

18 0.85) and lesions with %AS <58% and maximum TAWSS <7.69 Pa had a long-term prevalence

19 of lesion-oriented events below 6%.[26] Our study confirmed similar predictive cutoffs for both

20 %AS (55.5%) and maximum TAWSS (7.30 Pa).

1   These findings highlight the potential usefulness of the current approach in stratifying

2   mild lesions, hence tailoring preventive therapeutic strategies in patients without

3   hemodynamically significant lesions.

4   *Emerging role of TSVI*

5   WSS topological skeleton features identify blood flow stagnation, recirculation and

6   separation regions,[27] previously identified as flow disturbances promoting atherosclerosis.[12]

7   Among WSS topological skeleton features, TSVI was initially associated with development of

8   long-term re-stenosis after carotid endarterectomy in humans[8]. Recently, TSVI has been linked

9   with early atherosclerotic changes in coronary arteries in preclinical swine models.[10] Of note,

10   high TSVI not only co-localized with higher wall thickness, but also predicted wall thickening

11   longitudinally.[10]

12   Based on these recent findings, this is the first study investigating the link between

13   TSVI and MI. More specifically, TSVI quantifies the variability in the contraction/expansion

14   action exerted by the WSS on the endothelium along the cardiac cycle. [8, 17] Translating this into

15   mechanistic implications, high WSS contraction/expansion variability, inducing endothelial

16   intra- and intercell tension variability, might promote shrinking/widening of cellular gaps,[27]

17   fibrous cap fragility, accelerated disease progression, up to plaque rupture with impact on

18   clinical outcomes.[4] This hypothesis, although warranting further investigation, is grounded on

19   the predictive capacity for MI of TSVI at the lesion level and downstream of the lesion in the

20   present study (**Supplemental Table 2**). Moreover, among 60 lesions with %AS, ΔvFFR and

21   TSVI above the threshold values, 45 (75%) evolved into a MI (**Supplemental Figure 11**). This

22   enhanced discrimination for plaques vulnerable to rupture or, conversely, prone to senescence

1   may provide the foundations for future clinical studies addressing different therapeutics

2   strategies in this subgroup of patients. Of note, the best predictive performance was achieved

3   by TSVI in predicting STEMI at 5 years (AUC 0.83, 95%CI 0.73-0.93, p<0.001).

4   Taken together with the previous evidences current results support the role of the WSS

5   contraction/expansion action along the cardiac cycle in promoting biological events, including

6   plaque formation, progression[8, 17] and, ultimately, destabilization. However, TSVI-associated

7   changes in plaque characteristic remains to be elucidated.

8

1   **Limitations**

2   This study has several limitations. First, the small number of patients included in the

3   final analysis. While explained by selection criteria of the retrospective screening, selection

4   biases cannot be excluded. Second, the retrospective study design limited our ability of

5   controlling for potential confounding factors, e.g. administration of intracoronary nitroglycerin

6   before image acquisition. Third, no information on plaque burden or composition are available.

7   Fourth, the uncertainty and the level of idealization inherent in the 3D reconstruction and the

8   CFD modelling might influence the considered WSS-based descriptors. In particular, the lack

9   of personalized flow measurements and the assumptions made to manage the inflow boundary

10   conditions could affect the WSS estimation. However, the use of generic Doppler velocity

11   curves scaled to fit patient-specific inlet cross-section diameter was previously validated in

12   vessels presenting luminal cross sectional area reduction $< 50\%$.[28] Moreover, in ongoing

13   analyses on diseased coronary arteries with available Doppler and frame count data, TSVI

14   resulted only modestly affected by the adoption of the boundary conditions applied in the

15   present study. Analytically, a possible explanation for this can be found in the use of the

16   normalized WSS vector in TSVI (see Eq.1).

1 **Conclusions**

2   The present study demonstrated (i) the value of CFD derived from conventional

3 coronary angiography and performed by clinicians and (ii) the capability of WSS-based

4 quantities to detect lesions culprit for future MI.

5   Although angiography-derived anatomical lesion severity and pressure drop along the

6 vessel showed capacity in identifying coronary lesions leading to MI, the extension of the

7 functional evaluation to include angiographic derived endothelial shear stress features

8 – TAWSS and TSVI – improved the predictive capacity for MI. TAWSS, the most common

9 WSS-based descriptor, was able to identify culprit lesions of a future MI, but with a modest

10 predictive capacity. In contrast, high TSVI showed to portray a five-fold increase in the risk

11 prediction for MI. Further clinical trials are required to translate these concepts into clinical

12 practice.

13

13 **Authors contribution**

1   **References**

2   1.   Kok AM, Molony DS, Timmins LH, Ko YA, Boersma E, Eshtehardi P, Wentzel JJ,

3   Samady H. The influence of multidirectional shear stress on plaque progression and

4   composition changes in human coronary arteries. EuroIntervention 2019;**15**(8):692-699.

5   2.   Wentzel JJ, Schuurbiers JC, Gonzalo Lopez N, Gijsen FJ, van der Giessen AG, Groen

6   HC, Dijkstra J, Garcia-Garcia HM, Serruys PW. In vivo assessment of the relationship between

7   shear stress and necrotic core in early and advanced coronary artery disease. EuroIntervention

8   2013;**9**(8):989-95; discussion 995.

9   3.   De Bruyne B, Pijls NH, Kalesan B, Barbato E, Tonino PA, Piroth Z, Jagic N, Mobius-

10   Winkler S, Rioufol G, Witt N, Kala P, MacCarthy P, Engstrom T, Oldroyd KG, Mavromatis

11   K, Manoharan G, Verlee P, Frobert O, Curzen N, Johnson JB, Juni P, Fearon WF, Investigators

12   FT. Fractional flow reserve-guided PCI versus medical therapy in stable coronary disease. N

13   Engl J Med 2012;**367**(11):991-1001.

14   4.   Chatzizisis YS, Coskun AU, Jonas M, Edelman ER, Feldman CL, Stone PH. Role of

15   endothelial shear stress in the natural history of coronary atherosclerosis and vascular

16   remodeling: molecular, cellular, and vascular behavior. J Am Coll Cardiol 2007;**49**(25):2379-

17   93.

18   5.   Puri R, Leong DP, Nicholls SJ, Liew GY, Nelson AJ, Carbone A, Copus B, Wong DT,

19   Beltrame JF, Worthley SG, Worthley MI. Coronary artery wall shear stress is associated with

20   endothelial dysfunction and expansive arterial remodelling in patients with coronary artery

21   disease. EuroIntervention 2015;**10**(12):1440-8.

1 6.   Kumar A, Hung OY, Piccinelli M, Eshtehardi P, Corban MT, Sternheim D, Yang B,

2 Lefieux A, Molony DS, Thompson EW, Zeng W, Bouchi Y, Gupta S, Hosseini H, Raad M,

3 Ko YA, Liu C, McDaniel MC, Gogas BD, Douglas JS, Quyyumi AA, Giddens DP, Veneziani

4 A, Samady H. Low Coronary Wall Shear Stress Is Associated With Severe Endothelial

5 Dysfunction in Patients With Nonobstructive Coronary Artery Disease. JACC Cardiovasc

6 Interv 2018;**11**(20):2072-2080.

7 7.   Kumar A, Thompson EW, Lefieux A, Molony DS, Davis EL, Chand N, Fournier S,

8 Lee HS, Suh J, Sato K, Ko YA, Molloy D, Chandran K, Hosseini H, Gupta S, Milkas A, Gogas

9 B, Chang HJ, Min JK, Fearon WF, Veneziani A, Giddens DP, King SB, 3rd, De Bruyne B,

10 Samady H. High Coronary Shear Stress in Patients With Coronary Artery Disease Predicts

11 Myocardial Infarction. J Am Coll Cardiol 2018;**72**(16):1926-1935.

12 8.   Morbiducci U, Mazzi V, Domanin M, De Nisco G, Vergara C, Steinman DA, Gallo D.

13 Wall Shear Stress Topological Skeleton Independently Predicts Long-Term Restenosis After

14 Carotid Bifurcation Endarterectomy. Ann Biomed Eng 2020.

15 9.   De Nisco G, Tasso P, Calo K, Mazzi V, Gallo D, Condemi F, Farzaneh S, Avril S,

16 Morbiducci U. Deciphering ascending thoracic aortic aneurysm hemodynamics in relation to

17 biomechanical properties. Med Eng Phys 2020;**82**:119-129.

18 10.   Mazzi V, De Nisco G, Hoogendoorn A, Calo K, Chiastra C, Gallo D, Steinman DA,

19 Wentzel JJ, Morbiducci U. Early Atherosclerotic Changes in Coronary Arteries are Associated

20 with Endothelium Shear Stress Contraction/Expansion Variability. Ann Biomed Eng 2021.

21 11.   Masdjedi K, van Zandvoort LJC, Balbi MM, Gijsen FJH, Ligthart JMR, Rutten MCM,

22 Lemmert ME, Wilschut J, Diletti R, De Jaegere P, Zijlstra F, Van Mieghem NM, Daemen J.

Validation of 3-Dimensional Quantitative Coronary Angiography based software to calculate Fractional Flow Reserve: Fast Assessment of STenosis severity (FAST)-study. EuroIntervention 2019.

12. Gijsen F, Katagiri Y, Barlis P, Bourantas C, Collet C, Coskun U, Daemen J, Dijkstra J, Edelman E, Evans P, van der Heiden K, Hose R, Koo BK, Krams R, Marsden A, Migliavacca F, Onuma Y, Ooi A, Poon E, Samady H, Stone P, Takahashi K, Tang D, Thondapu V, Tenekecioglu E, Timmins L, Torii R, Wentzel J, Serruys P. Expert recommendations on the assessment of wall shear stress in human coronary arteries: existing methodologies, technical considerations, and clinical applications. Eur Heart J 2019;**40**(41):3421-3433.

13. Ku DN, Giddens DP, Zarins CK, Glagov S. Pulsatile flow and atherosclerosis in the human carotid bifurcation. Positive correlation between plaque location and low oscillating shear stress. Arteriosclerosis 1985;**5**(3):293-302.

14. Peiffer V, Sherwin SJ, Weinberg PD. Computation in the rabbit aorta of a new metric - the transverse wall shear stress - to quantify the multidirectional character of disturbed blood flow. J Biomech 2013;**46**(15):2651-8.

15. Morbiducci U, Gallo D, Cristofanelli S, Ponzini R, Deriu MA, Rizzo G, Steinman DA. A rational approach to defining principal axes of multidirectional wall shear stress in realistic vascular geometries, with application to the study of the influence of helical flow on wall shear stress directionality in aorta. J Biomech 2015;**48**(6):899-906.

16. Himburg HA, Grzybowski DM, Hazel AL, LaMack JA, Li XM, Friedman MH. Spatial comparison between wall shear stress measures and porcine arterial endothelial permeability. Am J Physiol Heart Circ Physiol 2004;**286**(5):H1916-22.

1   17.   Mazzi V, Gallo D, Calo K, Najafi M, Khan MO, De Nisco G, Steinman DA,

2   Morbiducci U. A Eulerian method to analyze wall shear stress fixed points and manifolds in

3   cardiovascular flows. Biomech Model Mechanobiol 2020;**19**(5):1403-1423.

4   18.   DeLong ER DDaC-PD. Comparing the Areas under Two or More Correlated Receiver

5   Operating Characteristic Curves: A Nonparametric Approach. Biometrics 1988;**Vol. 44, No. 3**

6   **(Sep., 1988), pp. 837-845**.

7   19.   Naghavi M, Libby P, Falk E, Casscells SW, Litovsky S, Rumberger J, Badimon JJ,

8   Stefanadis C, Moreno P, Pasterkamp G, Fayad Z, Stone PH, Waxman S, Raggi P, Madjid M,

9   Zarrabi A, Burke A, Yuan C, Fitzgerald PJ, Siscovick DS, de Korte CL, Aikawa M, Juhani

10 Airaksinen KE, Assmann G, Becker CR, Chesebro JH, Farb A, Galis ZS, Jackson C, Jang IK,

11 Koenig W, Lodder RA, March K, Demirovic J, Navab M, Priori SG, Rekhter MD, Bahr R,

12 Grundy SM, Mehran R, Colombo A, Boerwinkle E, Ballantyne C, Insull W, Jr., Schwartz RS,

13 Vogel R, Serruys PW, Hansson GK, Faxon DP, Kaul S, Drexler H, Greenland P, Muller JE,

14 Virmani R, Ridker PM, Zipes DP, Shah PK, Willerson JT. From vulnerable plaque to

15 vulnerable patient: a call for new definitions and risk assessment strategies: Part I. Circulation

16 2003;**108**(14):1664-72.

17 20.   Stone GW, Maehara A, Lansky AJ, de Bruyne B, Cristea E, Mintz GS, Mehran R,

18 McPherson J, Farhat N, Marso SP, Parise H, Templin B, White R, Zhang Z, Serruys PW,

19 Investigators P. A prospective natural-history study of coronary atherosclerosis. N Engl J Med

20 2011;**364**(3):226-35.

21 21.   Johnson TW, Raber L, Di Mario C, Bourantas CV, Jia H, Mattesini A, Gonzalo N, de

22 la Torre Hernandez JM, Prati F, Koskinas KC, Joner M, Radu MD, Erlinge D, Regar E,

1   Kunadian V, Maehara A, Byrne RA, Capodanno D, Akasaka T, Wijns W, Mintz GS,

2   Guagliumi G. Clinical use of intracoronary imaging. Part2: acute coronary syndromes,

3   ambiguous coronary angiography findings, and guiding interventional decision-making: an

4   expert consensus document of the European Association of Percutaneous Cardiovascular

5   Interventions. EuroIntervention 2019;**15**(5):434-451.

6   22.   Lee JM, Choi G, Koo BK, Hwang D, Park J, Zhang J, Kim KJ, Tong Y, Kim HJ, Grady

7   L, Doh JH, Nam CW, Shin ES, Cho YS, Choi SY, Chun EJ, Choi JH, Norgaard BL,

8   Christiansen EH, Niemen K, Otake H, Penicka M, de Bruyne B, Kubo T, Akasaka T, Narula

9   J, Douglas PS, Taylor CA, Kim HS. Identification of High-Risk Plaques Destined to Cause

10   Acute Coronary Syndrome Using Coronary Computed Tomographic Angiography and

11   Computational Fluid Dynamics. JACC Cardiovasc Imaging 2019;**12**(6):1032-1043.

12   23.   Stone PH, Coskun AU, Kinlay S, Popma JJ, Sonka M, Wahle A, Yeghiazarians Y,

13   Maynard C, Kuntz RE, Feldman CL. Regions of low endothelial shear stress are the sites where

14   coronary plaque progresses and vascular remodelling occurs in humans: an in vivo serial study.

15   Eur Heart J 2007;**28**(6):705-10.

16   24.   Samady H, Eshtehardi P, McDaniel MC, Suo J, Dhawan SS, Maynard C, Timmins LH,

17   Quyyumi AA, Giddens DP. Coronary artery wall shear stress is associated with progression

18   and transformation of atherosclerotic plaque and arterial remodeling in patients with coronary

19   artery disease. Circulation 2011;**124**(7):779-88.

20   25.   Bourantas CV, Zanchin T, Torii R, Serruys PW, Karagiannis A, Ramasamy A, Safi H,

21   Coskun AU, Koning G, Onuma Y, Zanchin C, Krams R, Mathur A, Baumbach A, Mintz G,

22   Windecker S, Lansky A, Maehara A, Stone PH, Raber L, Stone GW. Shear Stress Estimated

1   by Quantitative Coronary Angiography Predicts Plaques Prone to Progress and Cause Events.

2   JACC Cardiovasc Imaging 2020;**13**(10):2206-2219.

3   26.   Tufaro V SH, Torii R, Koo BK, Kitslaar P, Ramasamy A, Mathur A, Jones DA, Bajaj

4   R, Erdoğan E, Lansky A, Zhang J, Konstantinou K, Little CD, Rakhit R, Karamasis GV,

5   Baumbach A, Bourantas CV. Wall shear stress estimated by 3D-QCA can predict

6   cardiovascular events in lesions with borderline negative fractional flow reserve.

7   Atherosclerosis 2021(02.018).

8   27.   Melchior B, Frangos JA. Shear-induced endothelial cell-cell junction inclination. Am J

9   Physiol Cell Physiol 2010;**299**(3):C621-9.

10   28.   van der Giessen AG, Groen HC, Doriot PA, de Feyter PJ, van der Steen AF, van de

11   Vosse FN, Wentzel JJ, Gijsen FJ. The influence of boundary conditions on wall shear stress

12   distribution in patients specific coronary trees. J Biomech 2011;**44**(6):1089-95.

13

1   **Figures and legends to figures**
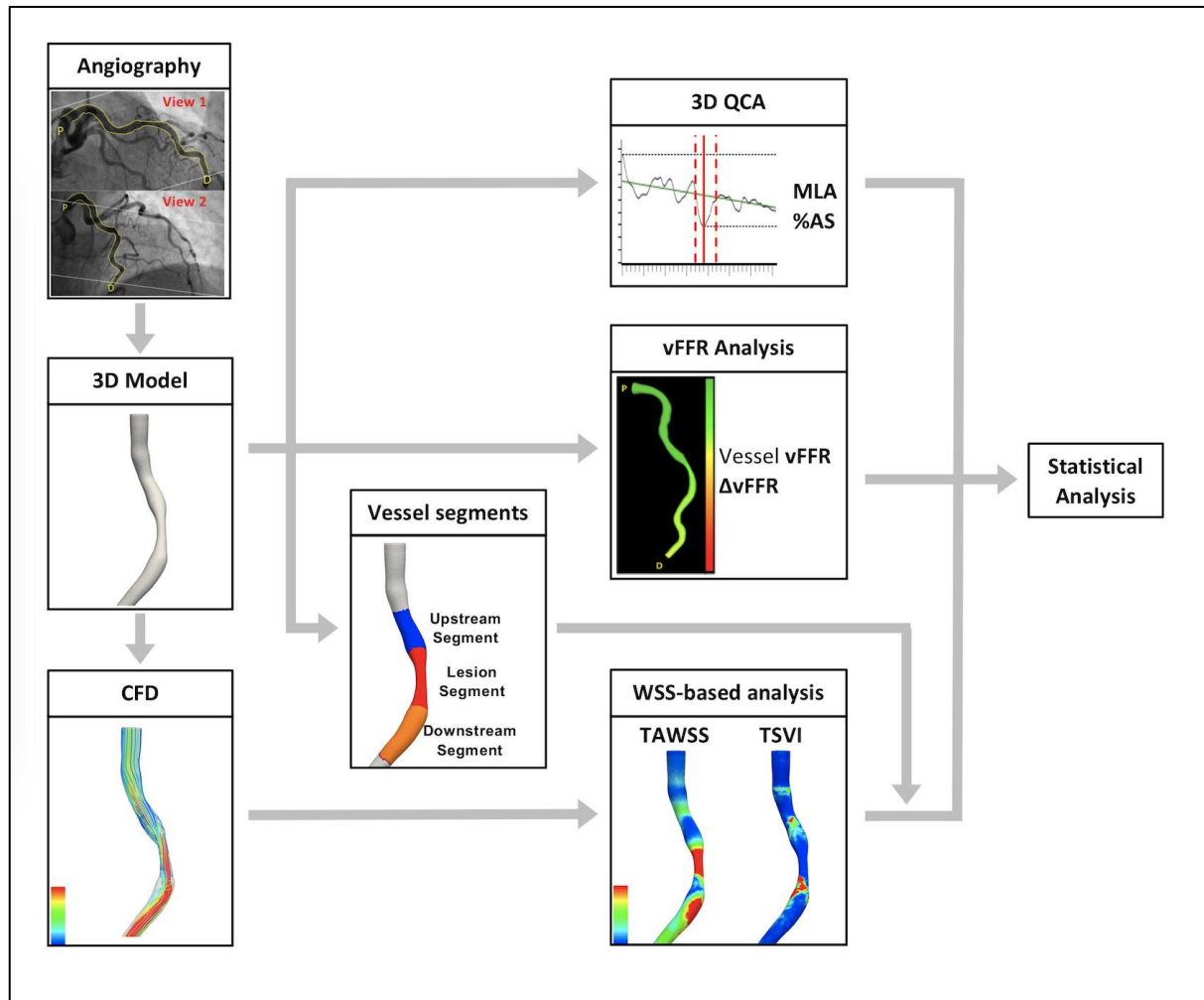
2

3   **Figure 1 – Workflow of the study.** The geometrical information of the three-dimensional

4   vessel reconstruction is exploited to compute in parallel quantitative coronary angiography

5   (QCA) analysis as well as virtual fractional flow reserve (vFFR) and computational fluid

6   dynamic (CFD)-derived wall shear stress (WSS) simulations.

7
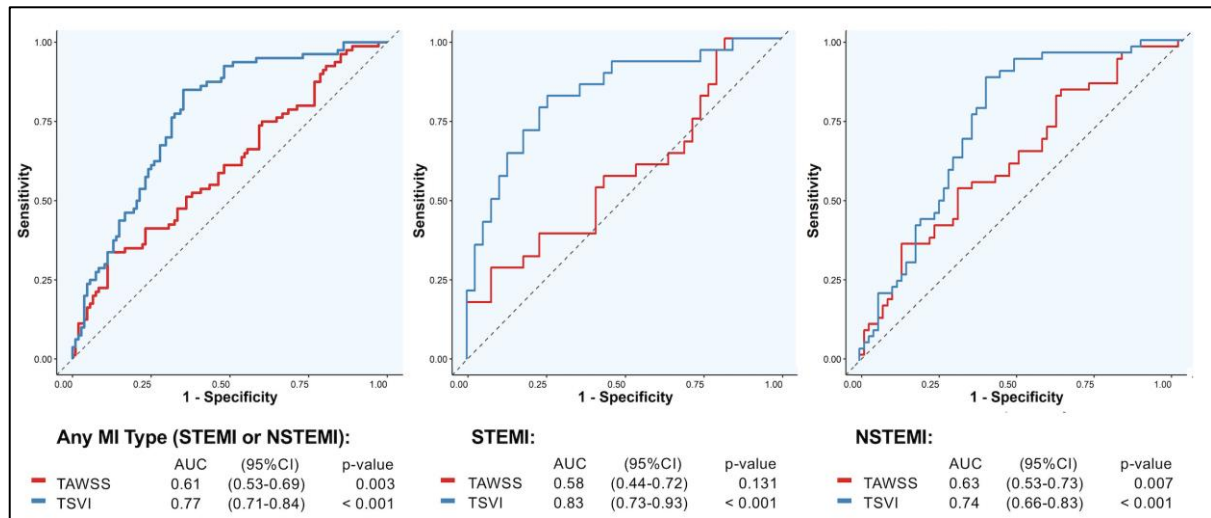
**Figure 2 – Receiver operating characteristic (ROC) curves of the adopted wall shear stress descriptors.** Topological shear variation index (TSVI) resulted in a good predictive capacity for any type of myocardial infarction (MI), which was significantly superior to the time-averaged wall shear stress (TAWSS). The best performance of TSVI was found in ST segment elevation myocardial infarction (STEMI).
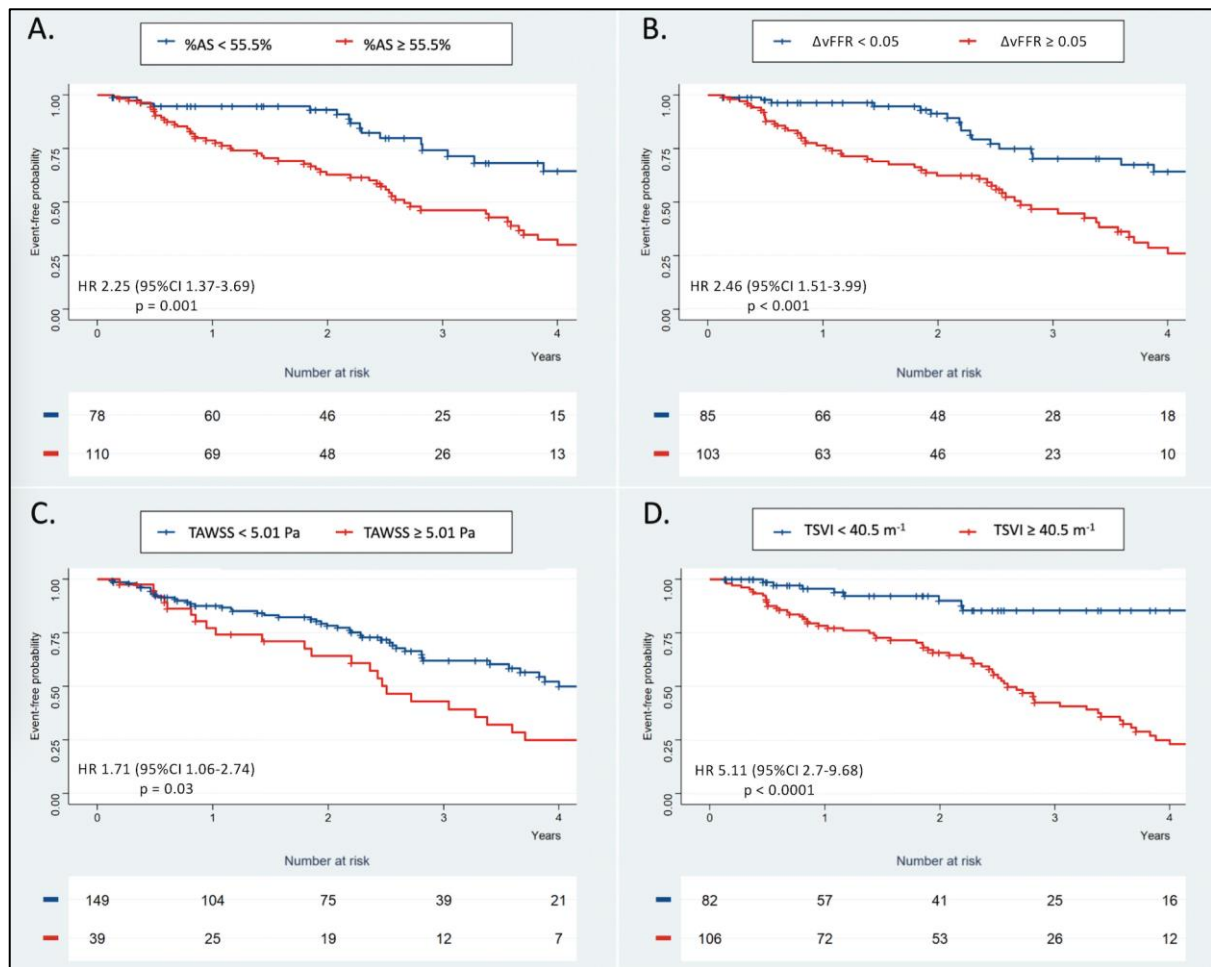
Figure 3 – Time-to-event curves. Significantly divergent Kaplan-Meier curves for future myocardial infarction are represented at 4-year follow-up for percentage area stenosis (%AS, panel A), translesional difference in virtual fractional flow reserve (ΔvFFR, panel B), lesion time-averaged wall shear stress (TAWSS, panel C) and lesion topological shear variation index (TSVI, panel D). Red and blue curves refer to values above or below the threshold values obtained from the ROC analysis, respectively. Hazard ratio (HR) refers to the whole follow-up time interval (i.e. 5 years).

1   **Text tables and legends to tables**

Table 1. Clinical characteristics (N= 80)	
Age, yrs	70.3 ±12.7
Female	23 (28.7%)
Type of MI	
- NSTEMI	52 (65.0%)
- STEMI	28 (35.0%)
Treatment	
- PCI	78 (97.5)
- CABG	1 (1.3%)
- Medical	1 (1.3%)
Time from baseline ICA, months	25.9 ± 17.7
- 1 ICA before MI, n	67 (83.7%)
- ≥ 2 ICA before MI, n	13 (16.3%)
Hypertension	61 (76.3%)
Hyperlipidaemia	63 (78.8%)
Diabetes mellitus	20 (25.0%)
- Insulin therapy	7 (8.8%)

Smoking	21(26.3%)
LVEF < 55%	18 (22.5%)
Reduced kidney function*	18 (22.5%)
Prior PCI	37 (46.3%)
Prior stroke	13 (16.3%)
Prior PVD	18 (22.5%)
Aspirin	61 (76.3%)
Statin	72 (90.0%)
P2Y12 inhibitors	15 (18.8%)

1

2   Clinical characteristics of the studied population at the time of the acute myocardial infarction

3   (index event). Coronary artery bypass graft, CABG; Invasive coronary angiography, ICA; Left

4   ventricle ejection fraction, LVEF; Myocardial infarction, MI; non-ST segment elevation

5   myocardial infarction, NSTEMI; Percutaneous coronary intervention, PCI; Peripheral vascular

6   disease, PVD; ST segment elevation myocardial infarction, STEMI. * eGFR < 60 ml/min/1.73

7   m2.

8

Table 2. Results of the quantitative coronary angiography (QCA) and the virtual fractional flow reserve (vFFR) analysis (Vessel N = 188)			
	Future culprit lesion (Vessel N = 80)	Non-culprit lesion (Vessel N = 108)	*p*-value
Vessel category			
RCA	22 (27.5%)	30 (27.8%)	0.928
LAD	35 (43.8%)	35 (32.4%)	0.184
LCX	23 (28.7%)	43 (39.8%)	0.207
Area stenosis, %	63.1±12.4	55.8±12.5	< 0.001
Diameter stenosis, %	40.2±10.6	34.3±9.66	< 0.001
Diameter stenosis			
<30%	15 (18.8%)	31 (28.7%)	0.118
≥30% and ≤50%	48 (60.0%)	72 (66.7%)	0.350
>50%	17 (21.2%)	5 (4.6%)	< 0.001
Minimal lumen area (MLA), mm^2	2.31±1.24	2.64±1.23	0.064
Minimal lumen diameter (MLD), mm	1.65±0.46	1.78±0.43	0.045
Reference vessel diameter, mm	2.78±0.63	2.74±0.62	0.668
Lesion length, mm	17.1 (IQR 11.8-26.0)	15.6 (IQR 10.3-28.3)	0.526
Distance MLA from ostium, mm	38.1 (IQR 25.2-54.3)	36.8 (IQR 23.7-55.7)	0.643
Distal pressure drop, mmHg	14.5 (IQR 9.0-22.5)	12.0 (IQR 8.0-16.0)	0.012
Distal vFFR	0.84 (IQR 0.75-0.90)	0.86 (IQR 0.82-0.92)	0.009
Distal vFFR ≤ 0.80	27 (33.8%)	10 (9.3%)	<0.001

ΔvFFR	0.08 (IQR 0.04-0.13)	0.05 (IQR 0.03-0.08)	0.002
Contour correction, %	9.5 (IQR 5.5-14.75)	10.2 (IQR 6.0-14.75)	0.486

1

2　Output of the quantitative coronary angiography (QCA) and virtual fractional flow reserve

3　(vFFR) according to the a priori known clinical classifier (culprit or nonculprit). Interquartile

4　range (IQR). ΔvFFR, translesional vFFR difference.

5